

A Numerical Model for Tri-Axially Braided Composites Under High Velocity Soft Projectile Impact

Jingyun Cheng, Wieslaw K. Binienda

*Department of Civil Engineering
The University of Akron, Akron OH*

Abstract

A simplified methodology has been developed for modeling 2D tri-axially braided composite plates impacted by a soft projectile using an explicit nonlinear finite element analysis code LS-DYNA. Fiber preform architecture is modeled using shell elements by incorporating the fiber preform architecture at the level of integration points. The soft projectile was modeled by an Equation of State (EOS). An arbitrary Lagrangian-Eulerian (ALE) formulation is used to resolve numerical problems caused by large projectile deformation. The computed results indicate that this numerical model is able to simulate a tri-axially braided composite undergoing a ballistic impact effectively and accurately, including the deformation and failure with a reasonable level of computational efficiency.

1. Introduction

Currently, 2D tri-axially braided polymer matrix composites are beginning to be widely used in the aerospace and automotive industry, especially for those structures where a high level of impact resistance is required. Compared with unidirectional composites, to form tri-axially braided composites three systems of yarns are intertwined diagonally. This fiber architecture offers an improved resistance to interlaminar cracking and delamination during impact. However, the geometrical parameters and material behavior of the composite such as the fiber architecture, fiber waviness, resin properties and the fiber/matrix interface affect the deformation behavior and failure mechanisms. Developing the ability to predict the mechanical properties and the impact response of braided composites is becoming an issue of interest in the research community. Chou[1] gave a detailed description of various textile composites and developed series methods to calculate the elastic constants of these materials. Flanagan [2] conducted a series of ballistic impact tests on two- and three- dimensionally woven and braided composites using a Lexan® right cylindrical projectile. The failure modes of the material, including indentation, matrix cracking, tensile and shear fiber failure and shear plugging, were categorized in terms of the velocity regime, the number and combination of material layers and types, and the debris mass. Beard [3] did crushing tests on 2D tri-axially braided composites tubes. The experimental results showed that the load - displacement curve and overall energy absorption could be significantly affected by the fiber perform architecture. The unit cell concept has been implemented by many researchers to investigate the mechanical properties of textile composites. Jiang[4] developed a methodology in which a plane weave woven composite was discretized into a series of four connected sub-cells. A through-the thickness homogenization process was then applied within the plane of the composite to compute the overall effective properties. Relatively little work has been done on 2D tri-axially braided composites due to the complex geometry. Quek[5] developed a micromechanical unit cell model to simulate 2D tri-axially braided composites, but the method used to approximate the axial tow inside this model made it hard to simulate the damage progression process accurately. Blankerhorn[6] used shell elements and solid elements to discretize the fiber tow of textile composites in a finite element analysis, with a contact formulation being used to simulate the interaction of the fiber tows both within a layer

and between layers. However, direct finite element meshing like that employed in this study is very time consuming due to the large number of element required.

Motivated by experimental results reported by Roberts [7], this study presents a discussion of a method to conduct numerical simulations of the deformation and failure response of 2D tri-axially braided composites under high velocity impact conditions. A preliminary analysis approach that was used to simulate the tri-axially braided materials is discussed in Cheng [8]. In these analyses, in which the transient dynamic, explicit finite element code LS-DYNA [9] was employed, to model the gelatin projectile a Lagrangian formulation was used along with an Equation of State (EOS) material model. Using this approach, it was possible to simulate the overall impact dynamics, the damage initiation threshold, and the penetration threshold. However, two improvements were found to be needed to improve the accuracy of the simulations. First, a more robust material model is needed for the gelatin projectile. Second, improvements in the composite material model are needed to fully account for the effect of fiber architecture on the direction and extent of crack propagation. With respect to the first issue, as will be described briefly in this paper, an Arbitrary Lagrangian Eulerian formulation has been implemented for the projectile. However, the major concern of the present paper is to describe the development of a simplified method for simulating the response of a 2D tri-axially braided composite under ballistic impact conditions. In this method, the geometry of the braided fiber tows is simulated by varying the fiber orientation of the composite at the different integration points in the finite element mesh both through the thickness of the ply and at various locations within the plane of the composite ply. Specifically, the unit cell of the 2D tri-axially braided composite is divided into four sub-cells, with each sub-cell consisting of fiber tows with varying size, fiber orientation and ply layup based on the actual geometrical shape and location. In the model, each fiber tow is modeled as if it is a unidirectional composite. By appropriate placement of the unit cells, the whole composite structure can be modeled. For this study, the effects of strain rate and the fiber/matrix interface are not considered. For this paper, the analytical method described above is utilized to simulate the ballistic impact response of a representative braided composite material with two different fiber perform architectures. In Section 2, the analytical method used to model the composite is described in detail, including the discretization methods used to model the fiber tows, and the techniques used to determine the material constants. Section 3 describes the material model used to model the gelatin projectile along with the details of the finite element analysis. Finally, Section 4 describes the numerical simulations that were performed, and comparisons between the experimental results and the numerical simulations are discussed.

2. Simplified Braiding through Thickness Integration Points Methodology

A very popular concept for material modeling of textile composites is unit cell micromechanical model. However, it has been found that it is very difficult to directly implement unit cell method in the 2D tri-axial composites. The main difficulties came from the following two sides. First, it was very difficult to mesh the unit cell with accurate geometry using commercial FEA preprocessor tools, especially the assurance of fiber volume ratio. Second, the unit cell size of 2D tri-axially braided composites was quite large so that micromechanical model of unit cell combined with homogenization may not capture the damage shape of 2D tri-axially braided composites during the impact. Therefore a simplified braided through thickness integration methodology has been proposed here to model 2D tri-axially braided composites. In this method, the geometry of the braided fiber tows was simulated by varying the fiber orientation of the

composite at the different integration points in the finite element mesh both through the thickness of the ply and at various locations within the plane of the composite ply. Specifically, the unit cell of the 2D tri-axially braided composite was divided into four sub-cells, with each sub-cell consisting of fiber tows with varying size, fiber orientation and ply layup based on the actual geometrical shape and location. In the model, each fiber tow was modeled as if it was a unidirectional composite. By appropriate placement of the unit cells, the whole composite structure can be modeled. In this study, the effects of strain rate and the fiber/matrix interface were not considered.

The detailed fiber architecture inside the unit cell of 2D tri-axial braid composites is shown in Figure 1 (a). In order to clearly illuminate the unit cell, the matrix material part is not shown in Figure 1 (a). The unit cell was divided into four Sub cells, in which sub-cell A consists of $\theta^\circ/0^\circ/-\theta^\circ$ fiber tow and matrix materials, sub-cell B consists of $\theta^\circ/-\theta^\circ$ fiber tow and matrix materials, sub-cell C consists of $-\theta^\circ/0^\circ/\theta^\circ$ fiber tow and matrix materials, and sub-cell D consists of $-\theta^\circ/\theta^\circ$ fiber tow and matrix materials, where θ is bias fiber braiding angle. The microstructure of 2D tri-axially braided composites is shown in Figure 2. Due to lack of microstructural geometry data of braided composites from the manufacturing company, Scanning Electron Microscopy (SEM) was used to measure the geometry of unit cell, which includes length, width, and thickness of fiber tows of different orientation angle. In order to reduce the measurement errors, data from several locations have been chosen and averaged. The dimensional data of fiber tows measured by Scanning Electron Microscopy (SEM) is listed in Table 1.

Table 1 The geometry of unit cell ($0^\circ/\pm 60^\circ$).

	Length (cm)	Width (cm)	Thickness (cm)
Sub-cell A	0.42	0.51	0.071
Sub-cell B	0.48	0.51	0.071
Sub-cell C	0.42	0.51	0.071
Sub-cell D	0.48	0.51	0.071

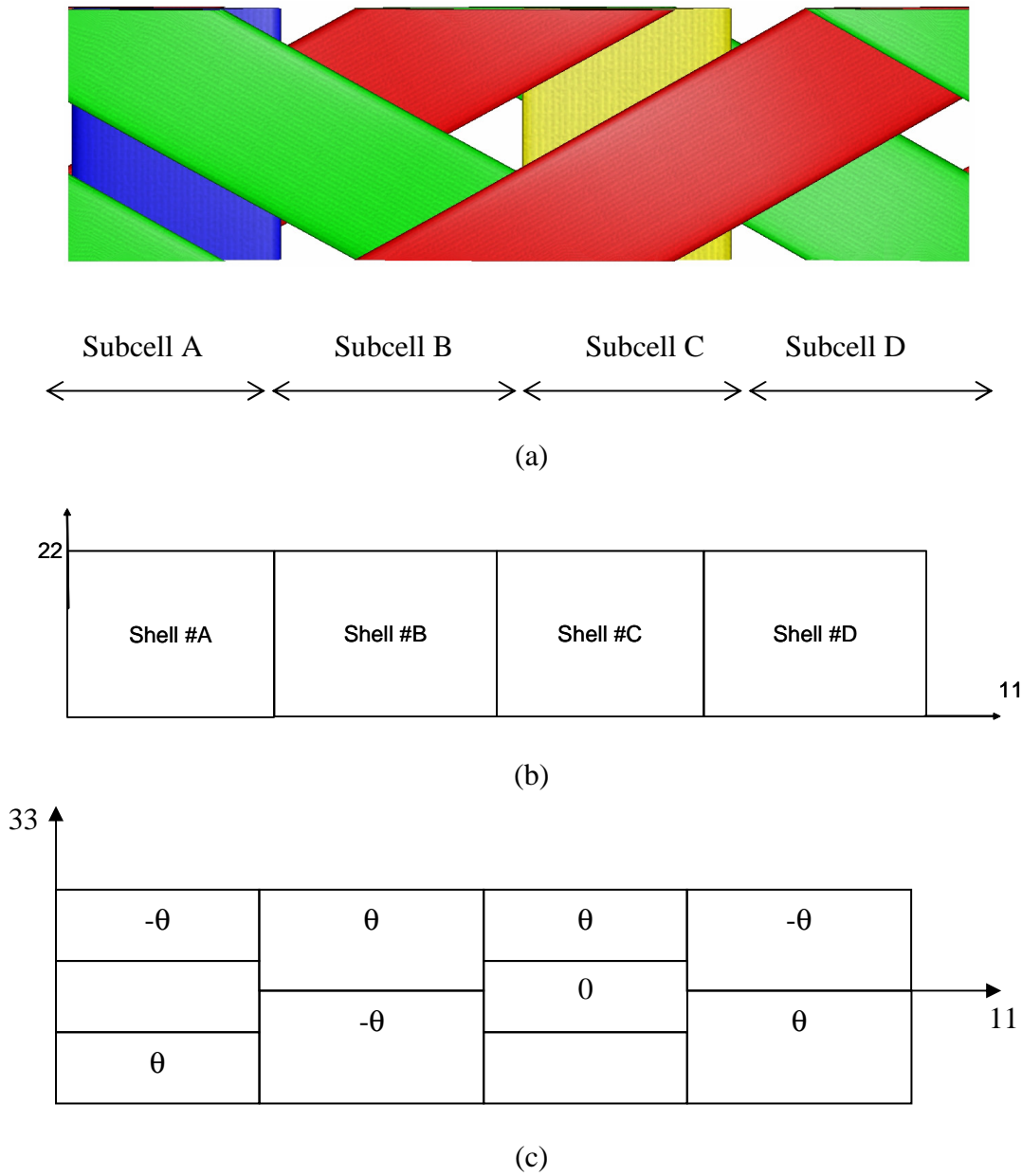


Figure 1 Schematic diagram of simplified braided through the thickness integration points methodology. (a) unit cell of tri-axially braided composites (fiber only), (b) mesh scheme of unit cell, (c) specification of fiber tow orientation angle at the through thickness integration points in one unit cell (1Ply) (11 and 22 are in-plane direction, 33 is the through the thickness direction).

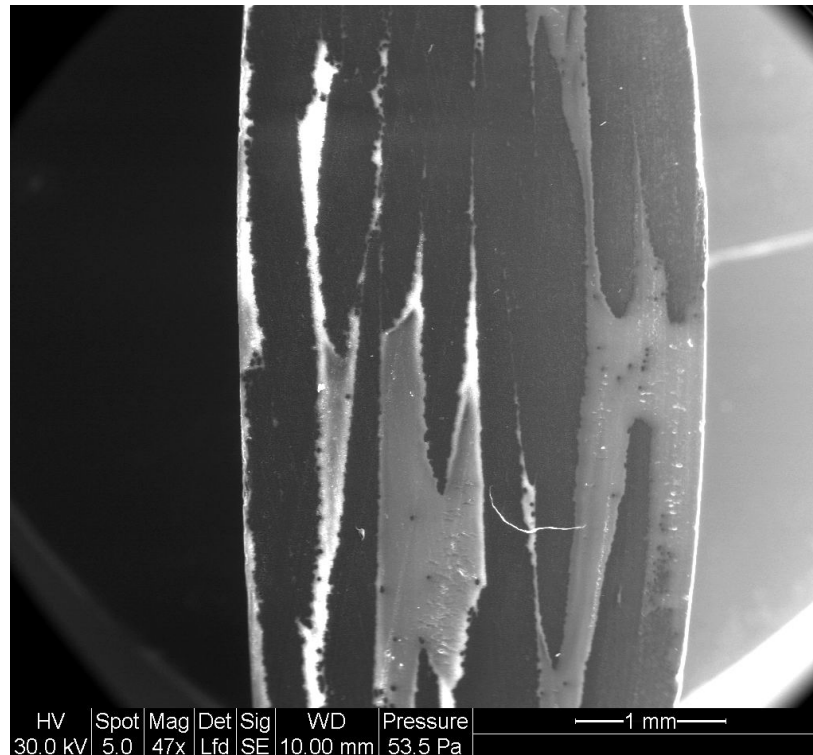


Figure 2 SEM image of 2D tri-axially braided composites.

Each sub-cell was modeled with layer composites using one shell element with several through the thickness integration points. Each different braiding angle fiber tow within this sub-cell was modeled as uni-directional composites through defining braiding angle at the corresponding integration point based on its stacking sequence. Four sub cells within one unit cell were modeled with four shell elements are shown in Figure 3. , in which braiding angle at through the thickness integration points was listed based on its location and stacking sequence. In LS-DYNA, Integration shell could be used to define layered composites through using the user defined integration rules, in which, each sub-cell is defined as a part consisted of different uni-directional composites with different orientation angle defined in its *SECTION_SHELL card. Appropriate used defined integration rule is used to assure the bending and membrane stiffness through using *INTEGRATION_SHELL card, where weight factor, and the thickness of each layer play an important rule, and each layer inside this card is defined as a 0 degree uni-directional composites referenced by a *PART card. For example, in sub-cell A, three parts are represented as θ° , 0° and $-\theta^\circ$ respectively in one ply. In sub-cell B, two parts are represented as $-\theta^\circ$, and θ° respectively in one ply. In sub-cell C, three parts are represented as $-\theta^\circ$, 0° and θ° respectively in one ply. In sub-cell D, two parts are represented as θ° , and $-\theta^\circ$ respectively in one ply. Therefore, the fiber tow size, fiber architecture and fiber undulation have been modeled by layered composites. Figure 3 shows the mesh scheme of a global structure and its relation with the unit cell. In this particular case the braided composites has 6 braided plies. So sub-cell A and sub-cell C need 18 integration points, sub-cell B and sub-cell D need only 12 integration points. Therefore, different materials represented by uni-directional composites with its orientation angle and its own material properties at the relevant integration point were interconnected with each other spatially, reproducing virtual 2D tri-axially braided composites.

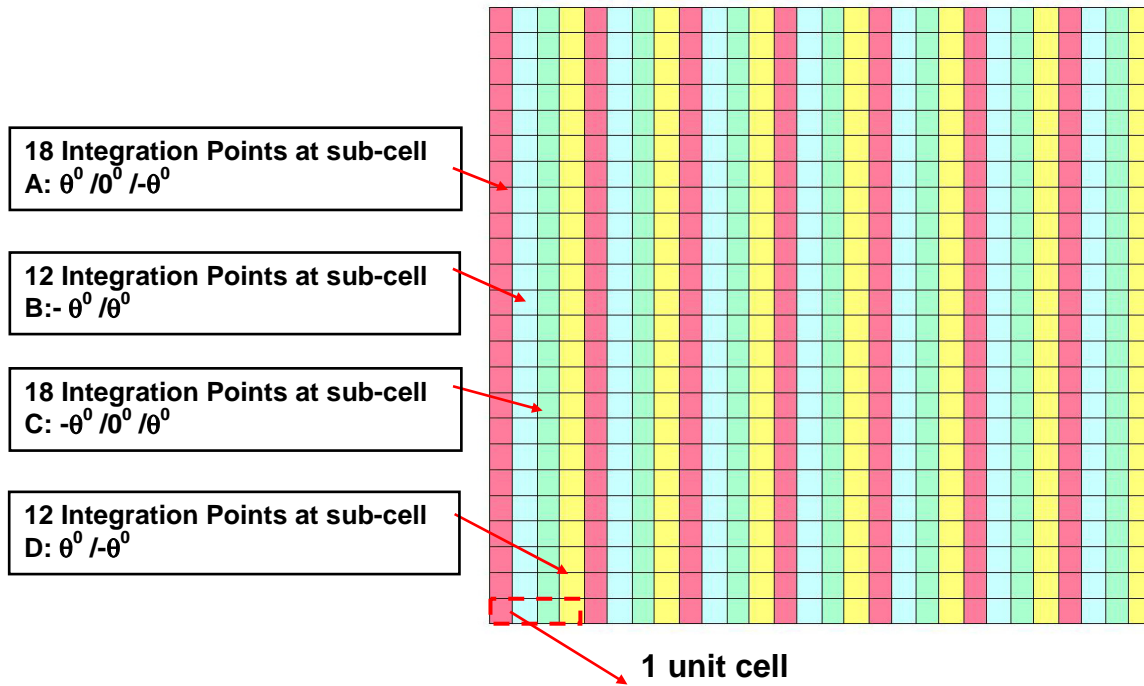


Figure 3 Meshing scheme of braiding through thickness integration points method.

Each part at different location of different sub-cell of 2D tri-axially braided composites has been approximated with uni-directional composites considering different fiber tow sizes and local bundle fiber volume ratio. Hence, the average fiber volume ratio of the entire composite is 60%. Based on SEM measured data, the bundle fiber volume ratio was calculated and is listed in Table 2.

Table 2 Fiber Volume Ratio of different fiber tow ($0^\circ/\pm 60^\circ$).

	0° Fiber Volume Ratio	60° Fiber Volume Ratio	-60° Fiber Volume Ratio
Sub-cell A	85%	62%	62%
Sub-cell B	n/a	50%	50%
Sub-cell C	85%	62%	62%
Sub-cell D	n/a	50%	50%

The corresponding material properties of uni-directional composites were calculated using the following equations:

$$E_x = V_f E_f + V_m E_m \quad (1)$$

$$\nu_x = V_f \nu_f + V_m \nu_m \quad (2)$$

$$\frac{1}{E_y} = \frac{V_f}{E_f} + \frac{V_m}{E_m} \quad (3)$$

$$\frac{1}{E_s} = \frac{V_f}{G_f} + \frac{V_m}{G_m} \quad (4)$$

$$\text{where } G_f = \frac{E_f}{2(1+\nu_f)} \text{ and } G_m = \frac{E_m}{2(1+\nu_m)} \quad (5)$$

where

E_x is the Young's modulus along the fiber 11 direction,

E_y is the Young's modulus in transverse 22 direction,

E_s is the in plane shear modulus, and

ν_x is the in plane Poisson's ratio,

V_f is the fiber volume ratio,

V_m is the matrix volume ratio,

E_f and E_m are the corresponding fiber and matrix Young's moduli,

ν_f and ν_m are the corresponding fiber and matrix Poisson's ratios,

G_f and G_m are the corresponding fiber and matrix shear moduli.

Here, fiber was assumed to be transverse isotropic, and matrix was assumed to be isotropic. The corresponding material properties used in this study are listed in Table 3. The Young's modulus, Poisson's ratio, tensile strength and failure strain of T700 fiber are obtained from the fiber producer - Toray, the value for transverse Young's modulus was taken from reference [10] based on representative carbon fiber data. The Young's modulus, Poisson's ratio and tensile strength of M36 Epoxy are from producer of the polymer - Hexply, and EPON 862, which was assumed to have similar properties as M36.

Table 3 Material properties of fiber and resin.

	Toray T700s Fiber	Hexply M36 Epoxy
Density (g/cm ³)	1.80	1.17
Young's modulus (Gpa)	230	3.5
Poisson ratio	0.23	0.42
Tensile Strength (Mpa)	4900	80
Failure Strain	2.1%	n/a

Maximum stress failure criteria was chosen for the unidirectional composite used for local laminate. There are four failure criteria:

Tensile fiber model (fiber rupture) $\sigma_{11} \geq 0$

$$e_f^2 = \left(\frac{\sigma_{11}}{X_t} \right)^2 - 1 \begin{cases} \geq 0 & \text{failed} \\ < 0 & \text{elastic} \end{cases} \quad (6)$$

When failed, the material is degraded through setting $E_a = E_b = G_{ab} = \nu_{ba} = \nu_{ab} = 0$

Compressive fiber model (fiber buckling and kinking) $\sigma_{11} < 0$

$$e_f^2 = \left(\frac{\sigma_{11}}{X_c} \right)^2 - 1 \begin{cases} \geq 0 & \text{failed} \\ < 0 & \text{elastic} \end{cases} \quad (7)$$

When failed, the material is degraded through $E_a = \nu_{ba} = \nu_{ab} = 0$

Tensile matrix mode (Matrix cracking under transverse tension and shearing)

$$e_m^2 = \left(\frac{\sigma_{22}}{Y_t} \right)^2 + \left(\frac{\tau}{S_c} \right)^2 - 1 \begin{cases} \geq 0 & \text{failed} \\ < 0 & \text{elastic} \end{cases} \quad (8)$$

When failed, the material is degraded through $E_b = \nu_{ab} = 0 \quad G_{ab} = 0$

Compressive matrix mode (Matrix cracking under transverse compression and shearing)

$$e_m^2 = \left(\frac{\sigma_{22}}{2S_c} \right)^2 + \frac{\sigma_{22}}{Y_c} \left[\frac{Y_c^2}{4S_c^2} - 1 \right] + \left(\frac{\tau}{S_c} \right)^2 - 1 \begin{cases} \geq 0 & \text{failed} \\ < 0 & \text{elastic} \end{cases} \quad (9)$$

When failed, the material is degraded through $E_b = \nu_{ba} = \nu_{ab} = 0 \quad G_{ab} = 0$

Here, X_t is tensile strength in 11 direction, X_c is compressive strength in 11 direction, Y_t is tensile strength in 22 direction, Y_c is compressive strength in 22 direction, and S_c is in plane shear strength.

Experimental results and theoretical research showed that tow strength depend on the number of the fiber and could be described using Weibull distribution. The main reason is that fiber interaction insider fiber bundle could weaken the strength. For example, the $0^\circ/\pm 60^\circ$ braided preform had 12k flat tow fibers in the $\pm 60^\circ$ (bias) directions and 24k flat tow fibers in the 0° (axial) direction, therefore, tensile strength of the 0° tow could be assumed to be 50% of the 60° and -60° bundles, because 0° tow contains twice as many fibers as $\pm 60^\circ$ tow.

Local failure is triggered by local stress at each integration point through checking all stress failure criteria. The material can be degraded at each integration point and each time step if one of the failure criteria is satisfied at any integration point.

3. Material Modeling of Gelatin and Arbitrary Lagrangian Eulerian (ALE) Formulation

Wilbeck gave a comprehensive description of impact by a soft projectile in his work [11]. When a soft projectile impacts a target plate, the particles on the front surface of the projectile are instantaneously brought to rest relative to the target and a shock wave is formed. The pressure in the shock region is very high initially and is constant throughout the region. As the shock propagates up the projectile, a very high pressure gradient is developing, and then a very complicated set of stress waves propagate in the projectile. Since the gelatin had a very low strength and stiffness, it can be described using the LS-DYNA Material 9 (MAT_NULL), in which the pressure-volume relation is modeled using the equation of state (EOS). This material model uses the equation of state without computing deviatoric stresses. The equation of state is defined by card *EOS_TABULATED where the pressure P is expressed as

$$P = C(\varepsilon_v) + \mathcal{A}(\varepsilon_v)E \quad (10)$$

Where ε_v is the volumetric strain given by the natural logarithm of the relative volume, E is internal energy. C , γ and T are corresponding material constants.

In this study, a set of proprietary material constants have been used in the numerical simulation.

Experimental results showed the gelatin flows during the impact process, and a conventional Lagrangian description of this kind of large deformation can induce severe mesh distortion. An arbitrary Lagrangian Eulerian (ALE) formulation was chosen for gelatin. The ALE formulation is based on the arbitrary movement of a reference domain [12].

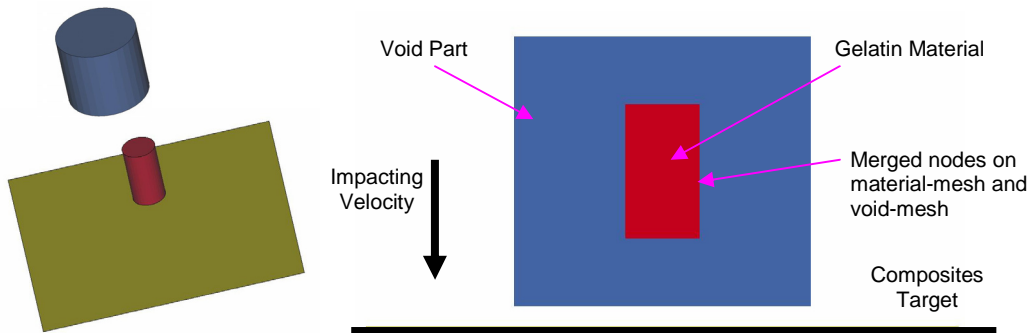


Figure4 ALE mesh scheme of gelatin impact on composites target.

In this application, the soft gelatin projectile was modeled with a multi-material Eulerian formulation through choosing solid element type (card *SECTION_SOLID, type 12), while the composite target was modeled with a Lagrangian formulation. Instead of contact in the pure Lagrangian formulation, a penalty-based ALE–Lagrangian coupling algorithm was chosen by using the card *CONSTRAINED_LAGRANGE_IN_SOLID. The meshes used to model the projectile, void part and the plate are shown in Figure 4. The validity of numerical results was examined by verifying the stability of the explicit finite element analysis through energy analysis and by comparing numerical results to the experimental data.

4. LS-DYNA Simulation Results and Discussion

Impact of the composite plate was simulated for velocities ranging from 91.4 m/s to 230 m/s. The penetration threshold for the $0^\circ/\pm 60^\circ$ flat panel was determined to be between 149.5 m/s and 154 m/s. Moreover, the penetration threshold for the $0^\circ/\pm 45^\circ$ flat panel was determined to be between 215 m/s and 218 m/s. These results are summarized in Table 4. It shows that the numerical simulation results agree well with experimental measurements.

Table 4 Penetration threshold velocity comparison.

	Penetration threshold velocity (m/s)	
	Experimental result	LSDYNA simulation
Flat Panel $0^\circ/\pm 60^\circ$	150 - 161	149.5 - 154
Flat Panel $0^\circ/\pm 45^\circ$	About 215m/s	215 - 218

Figure 5 shows the deformation behavior of both projectile and the impacted composites panels at the different stages. From the moment of impact, the projectile was gradually squashed into the panel and captured the pancake like shape, which was similar to that observed in high speed video of composite impact experiments.

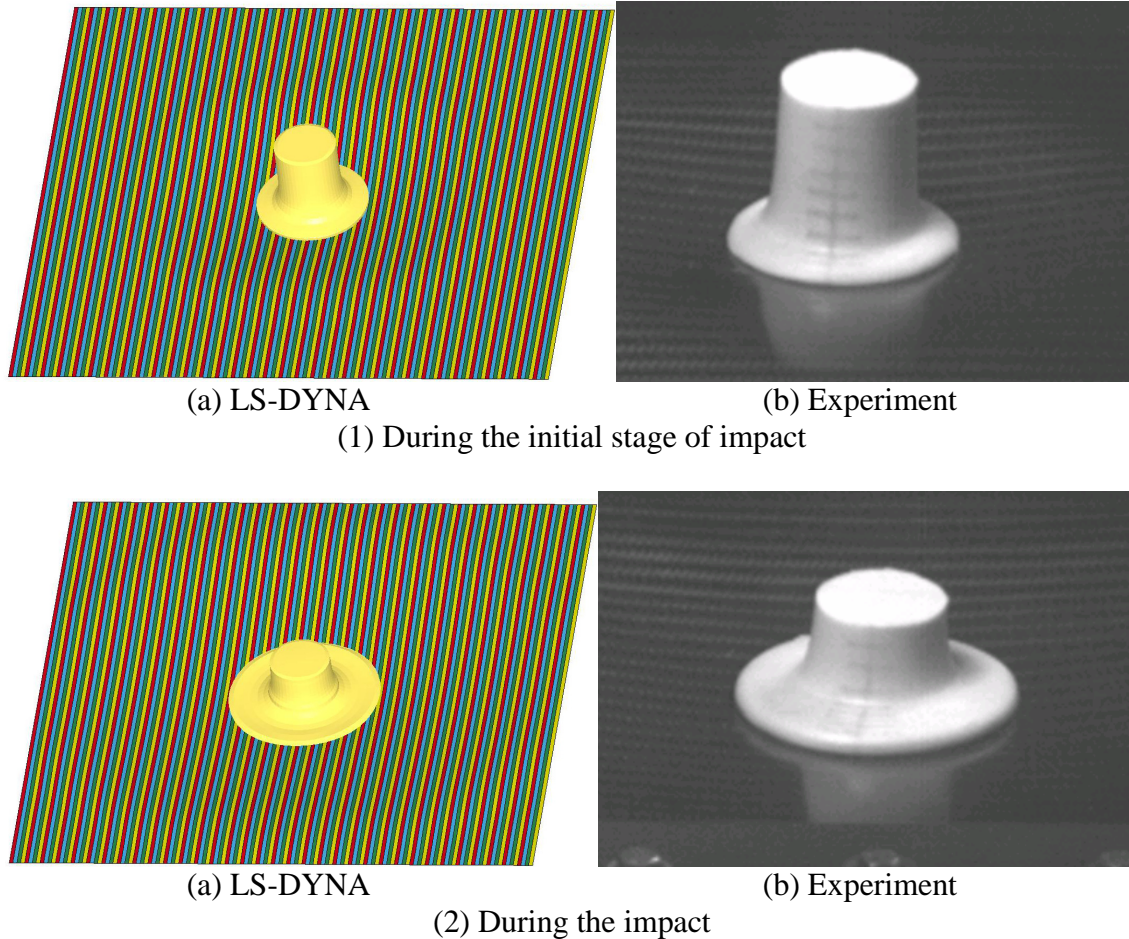


Figure 5 The deformation of gelatin and composites plate at the impact velocity of 128 m/s – LS-DYNA simulations and experiments.

Figure 6 shows the comparison of the out of plane displacement history of impact center taken from the numerical model with the experimental measurement by 3D image correlation photogrammetry ARAMIS system. The impact velocity was 128 m/s which was lower than penetration threshold. Comparison shows agreement between simulation and test from start till the center reach its maximum deformation and their respective maximum values were closed. Some discrepancy existed after the panel plate rebounded from the maximum out of plane displacement, when the panel was in its unloading stage.

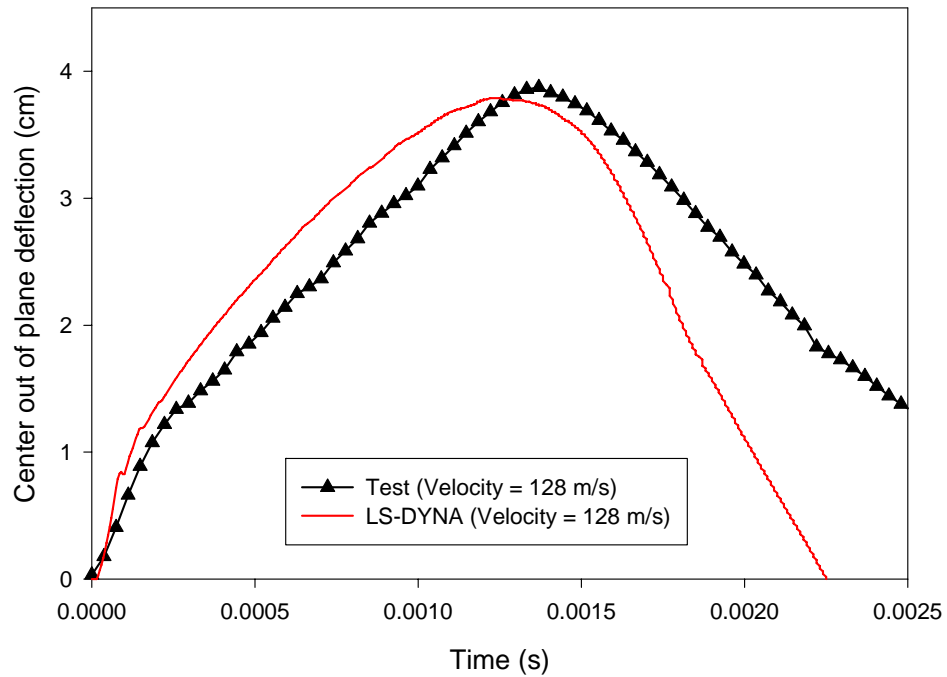


Figure 6 Center deflection of Epon 862[0°/±60°] braided composites plate.

In addition, the displacement from panel centerline has been exported. Figure 7 shows the panel at the impact velocity of 128 m/s. the displacement at different time has been compared. The comparisons show that the simulation results agree with the experimental measurements. It can be concluded that this method captures the main characteristics of deformation.

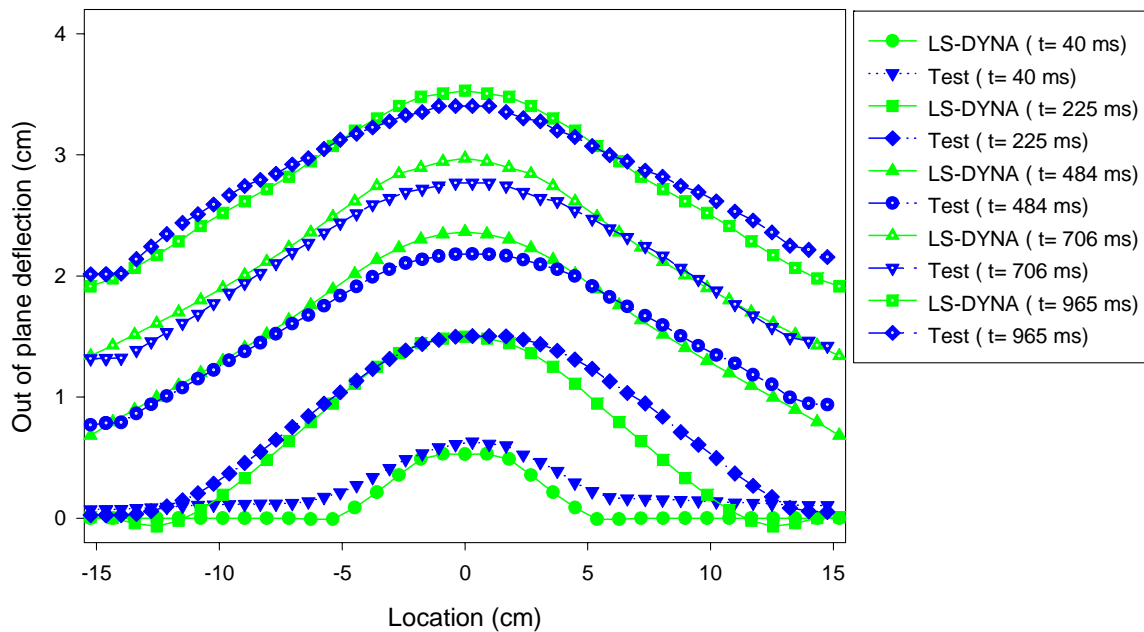


Figure 7 Out of plane deflection along a cross-section at the plate center under impact velocity of 128 m/s.

Figure 8 shows damage progression of M36[0°/±60°] flat panel during impact velocity of 192 m/s. The crack initiated at the location that was close to the impact center and grew symmetrically along ±60° degree directions and then along 0° direction. The final damage shape and size matched the experimental observation shown in Figure 9.

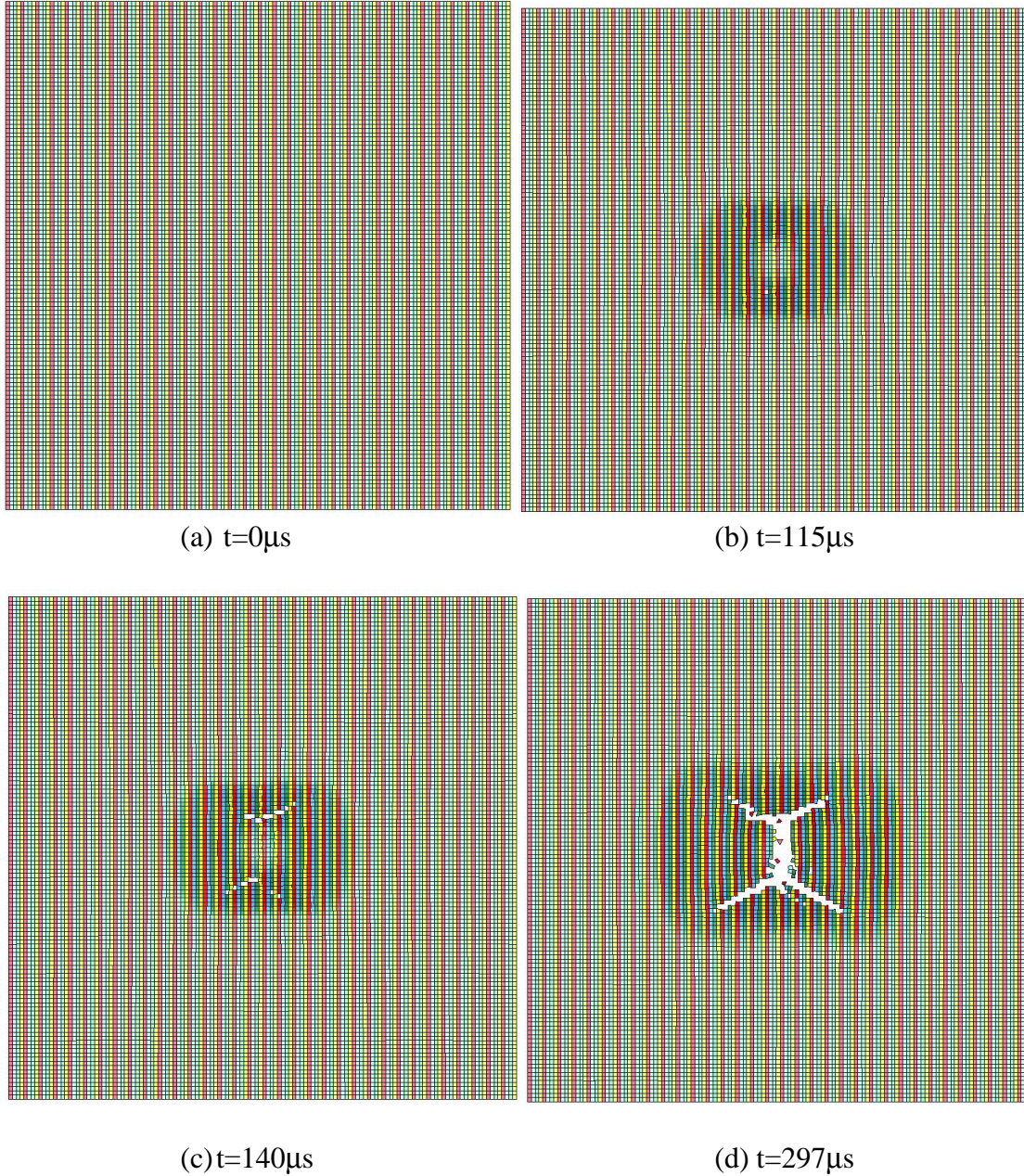


Figure 8 LS-DYNA simulation of damage pattern of M36[0°/±60°] at impact velocity 182 m/s.

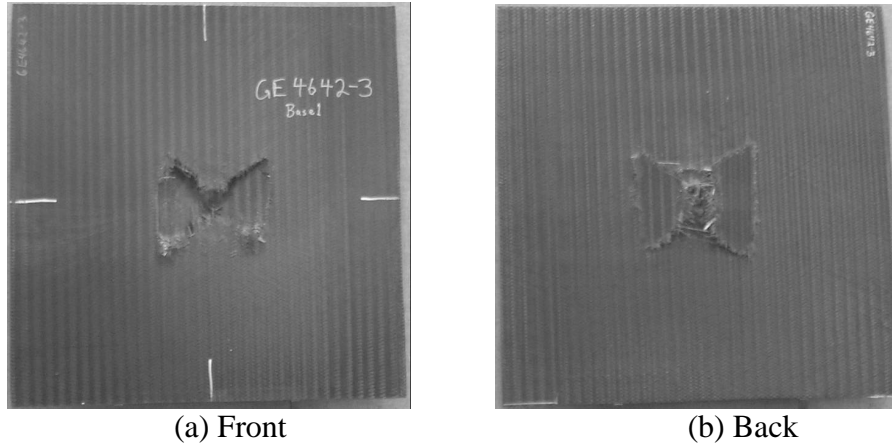


Figure 9 M36[0°/±60°] composites plate after impact at 192 m/s.

Figure 10 shows the numerical parametric study of damage progression of M36[0°/±45°] flat panel during impact velocity of 216 m/s. The cracks initiated at the center of plate and grew along 0° degree directions and then formed the final damage shape. The damage shape, size and its propagation sequence were all similar to the experimental observations shown in Figure 11.

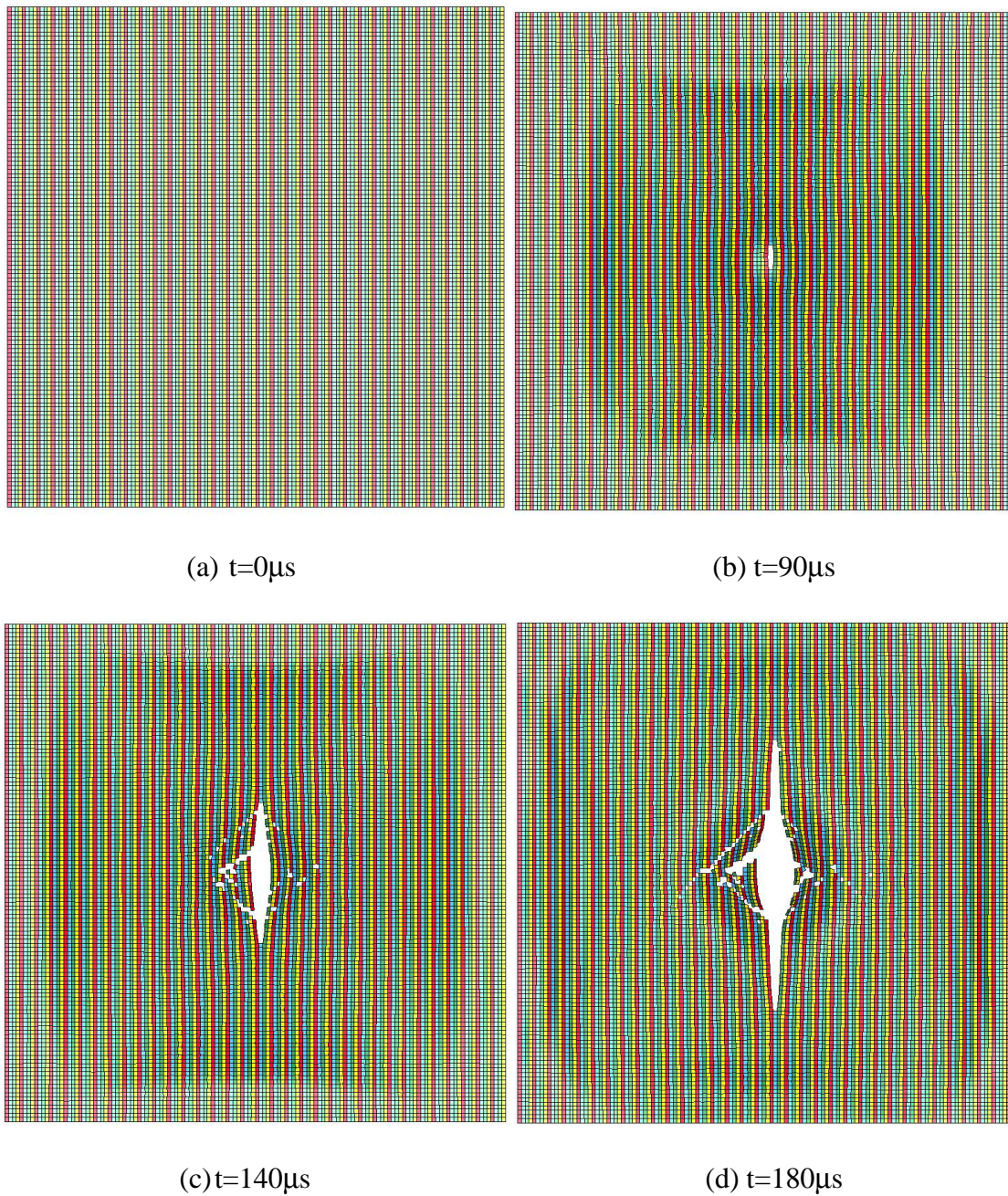


Figure 10 LS-DYNA simulation of damage pattern of M36[0°/±45°] at impact velocity 216 m/s.

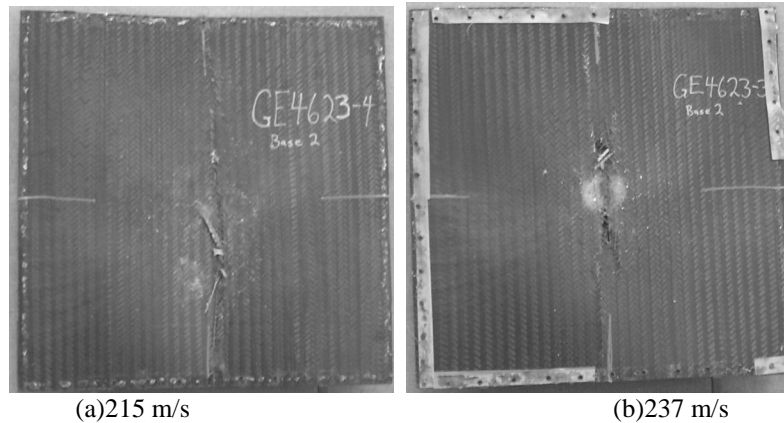


Figure 11 M36[0°/±45°] composites plate after impact

5. Conclusions

A simplified braiding through thickness integration points methodology has been proposed to model 2D tri-axial braided composites, this method considered the fiber tow size and fiber architecture inherently, as well as reduce calculation time dramatically. ALE formulation was used in this numerical simulation due to the large deformation of soft projectile. The numerical model was validated by ballistic impact test results. Numerical simulations showed this model captured the penetration threshold, deformation behavior and failure of two different fiber architecture 2D tri-axial braided composites. The agreement between numerical simulation and experimental results showed the potential use of this method in the real large structural impact analysis. Further investigation is needed to be implemented to fully understand this methodology, especially the effects of strain rate and fiber/matrix interface.

Acknowledgement

The authors would like to thank the NASA Glenn Research Center which funded part of this work through Contract No NCC3-932. and the technical assistance from Dr.Gary D.Roberts.

References

1. Chou T.W, and Ko F.K.: Textile Structural Composites. Volume 3 Composite Materials Series. Elsevier, 1989
2. Flanagan M.P, Zikry M.A, Will J.W and Shiekh A.El, An Experimental Investigation of High Velocity Impact and Penetration Failure Modes in Textile Composites. Journal of Composite Materials, Vol.33, No.12 1999, pp1080-1103.
3. Beard S and Chang F.K. Design of Braided Composites for Energy Absorption. Journal of Thermoplastic Composites Materials. Vol.15, Jan 2002, pp3-12.
4. Jiang Y, Tabiei, A.; and Simitse, G.J, A Novel Micromechanics-Based Approach to the Derivation of Constitutive Equations for Local/global Analysis of a Plain-Weave Composite. Composites Science and Technology, Vol. 60, pp. 1825-1833, 2000
5. Quek S.C, Waas A, Shahwan W.K and Agaram V. Compressive Response and Failure of Braided Textile Composites: Part 2-computations. Vol.39, 2004, pp 649-663.
6. Blankenhorn G, Schweizerhof K and Finckh H. Numerical Investigations of a Projectile Impact on a Textile Structure. 4th European LS-DYNA Conference. May 22-23, 2003, Ulm, Germany.

7. Roberts G.D, Pereira J.M, Revilock D.M, Binienda W.K, Xie M, and Braley M, Ballistic Impact of Composite Plates and Half-Rings with Soft Projectiles, 44th AIAA/ASME/ASCE/AHS Structures, Structural Dynamics, and Materials Conference, 7-10 April 2003, Norfolk, VA.
8. Cheng J, Roberts G.D and Binienda W.K. Finite Element Simulation of Soft Projectiles Impacting Composites Targets. SAMPE 2003. Dayton, OH.
9. LS-DYNA Keyword User's Manual Version 970, Livermore Software Technology Corporation, Livermore, CA, 2004.
10. Goldberg, R.K.: Implementation of Fiber Substructuring into Strain Rate Dependent Micromechanics Analysis of Polymer Matrix Composites. NASA/TM-2001-210822, 2001.
11. Wilbeck JS. Impact Behavior of Low Strength Projectiles. Ph.D. Dissertation. Texas A&M University. 1977.
12. Souli M, Ouahsine A and Lewin L. ALE Formulation for Fluid-Structure Interaction Problems. Comput. Methods Appl. Mech. Engrg. Vol.190,2000, pp659-675.